

Strong support for the millisecond pulsar origin of the Galactic center GeV excess

Richard Bartels,^{1,*} Suraj Krishnamurthy,^{1,†} and Christoph Weniger^{1,‡}

¹*GRAPPA Institute, University of Amsterdam, Science Park 904, 1090 GL Amsterdam, Netherlands*

(Dated: October 24, 2018)

Using γ -ray data from the *Fermi* Large Area Telescope, various groups have identified a clear excess emission in the inner Galaxy, at energies around a few GeV. This excess resembles remarkably well a signal from dark matter annihilation. One of the most compelling astrophysical interpretations is that the excess is caused by the combined effect of a previously undetected population of dim γ -ray sources. Due to their spectral similarity, the best candidates are millisecond pulsars. Here, we search for this hypothetical source population, using a novel approach based on wavelet decomposition of the γ -ray sky and the statistics of Gaussian random fields. Using almost seven years of *Fermi*-LAT data, we detect a clustering of photons as predicted for the hypothetical population of millisecond pulsar, with a statistical significance of 10.8σ . For plausible values of the luminosity function, this population explains 100% of the observed excess emission. We argue that other extragalactic or Galactic sources, a mismodeling of Galactic diffuse emission, or the thick-disk population of pulsars are unlikely to account for this observation.

Introduction. Since its launch in 2008, the *Fermi* Large Area Telescope (LAT) has revolutionized our understanding of the γ -ray sky. Among the major successes are the detection of more than three thousand γ -ray sources [1], the discovery of the *Fermi* bubbles [2], some of the most stringent limits on dark matter annihilation [3], and most recently the detection of cross-correlations between the extragalactic γ -ray background and various galaxy catalogues [4].

One of the most interesting γ -ray signatures, identified in the *Fermi*-LAT data by various groups [5–16], is an excess emission in the inner Galaxy at energies around a few GeV. This excess attracted great attention, because it has properties typical for a dark matter annihilation signal. This *Galactic center excess* (GCE) is detected both within the inner 10 arcmin of the Galactic center (GC) [7, 9, 10] and up to Galactic latitudes of more than ten degrees [13, 15, 17, 18]. It features a remarkably uniform spectrum and approximately spherical symmetry [13, 15]. Proposed diffuse emission mechanisms, like leptonic or hadronic outbursts [19–21] or cosmic-ray injection in the central molecular zone [22], potentially explain part of the excess emission. However, it is challenging to explain *all* of the above aspects of the GCE with these mechanisms alone.

The probably most plausible astrophysical interpretation for the GCE is the combined emission from a large number of unresolved millisecond pulsars (MSPs) in the Galactic bulge region [10, 12, 23, 24]. MSPs feature a spectrum compatible with the GCE emission [15], and a large unresolved component can naturally explain the uniformity of the GCE spectrum in different regions of the sky. Recently, it was shown that the spatial distribution of MSPs that were spilled out of disrupted globular clusters can explain the morphology of the GCE [25]. Further, though rather indirect, support for the MSP hypothesis comes from *Chandra* observation of low mass X-ray binaries (which are progenitor systems of MSPs)

in M31, which show a centrally peaked profile in the inner 2 kpc [26, 27], as well as the recent observation of extended hard X-ray emission from the Galactic center by *NuSTAR* [28].

It was claimed that an interpretation of 100% of the GCE emission in terms of MSPs would be already ruled out: A sizeable fraction of the required 10^3 – 10^4 MSPs should have been already detected by the *Fermi*-LAT [29, 30], but no (isolated) MSP has been identified so far in the bulge region. This conclusion depends, however, crucially on the adopted γ -ray luminosity of the brightest MSPs in the bulge population, on the effective source sensitivity of *Fermi*-LAT, and on the treatment of unassociated sources in the inner Galaxy [25, 31]. A realistic sensitivity study for MSPs in the context of the GeV excess, taking into account all these effects, was lacking in the literature up to now (but see Ref. [32]).

In this *Letter*, we close this gap and present a novel technique for the analysis of dim γ -ray sources, and apply it to *Fermi*-LAT observations of the inner Galaxy. Our method is based on the statistics of maxima in the wavelet-transformed gamma-ray sky.¹ We search for contributions from a large number of dim MSP-like sources, assuming that they are spatially distributed like suggested by GCE observations. Our method has several advantages w.r.t. previously proposed techniques based on one-point fluctuations [34], most notably the independence from Galactic diffuse emission models, and the ability for candidate source localization.

Modeling. We simulate a population of MSP-like sources, henceforth simply *central source population* (CSP), distributed around the GC at 8.5 kpc distance from the Sun. The CSP is taken to have a spatial distribution that follows a radial power-law with an index of

¹ In context of *Fermi*-LAT data, wavelet transforms were used previously for the identification of point source seeds [33].

$\Gamma = -2.5$ and a hard cutoff at radius $r = 3$ kpc [13, 15]. As reference γ -ray energy spectrum, we adopt the stacked MSP spectrum from Ref. [35], $\frac{dN}{dE} \propto e^{-E/3.78 \text{ GeV}} E^{-1.57}$. The γ -ray luminosity function is modeled with a power-law, $\frac{dN}{dL} \propto L^{-\alpha}$, with index $\alpha = -1.5$ [31, 35], and with lower and upper hard cutoffs at $L_{\min} = 10^{29} \text{ erg s}^{-1}$ and $L_{\max} = 10^{34}\text{--}10^{36} \text{ erg s}^{-1}$, respectively. Luminosities are integrated over 0.1–100 GeV. Our results depend little on L_{\min} . Given that only about 70 MSPs have been detected in γ -rays up to now [32], L_{\max} is not well constrained. The γ -ray luminosity of the brightest observed MSP is somewhere in the range $0.5\text{--}2 \cdot 10^{35} \text{ erg s}^{-1}$ [32, 35], depending on the adopted source distance [25, 31]. Diffuse emission is modeled with the standard model for point source analysis, `gll_iem_v06.fits`, and the corresponding isotropic background.

Data. For our analysis, we use almost seven years of ultraclean *Fermi*-LAT P8R2 data, taken between 4 Aug 2008 and 3 Jun 2015. We select both front and back converted events in the energy range 1–4 GeV, which covers the peak of the GCE spectrum. The Region Of Interest (ROI) covers the inner Galaxy and spans Galactic longitudes $|\ell| \leq 12^\circ$ and latitudes $2^\circ \leq |b| \leq 12^\circ$. The data is binned in Cartesian coordinates with a pixel size of 0.1° .

Wavelet peaks. The wavelet transform of the γ -ray data is defined as the convolution of the photon count map, $\mathcal{C}(\Omega)$, with the wavelet kernel, $\mathcal{W}(\Omega)$,

$$\mathcal{F}_{\mathcal{W}}[\mathcal{C}](\Omega) \equiv \int d\Omega' \mathcal{W}(\Omega - \Omega') \mathcal{C}(\Omega'), \quad (1)$$

where Ω denotes Galactic coordinates (note that $\int d\Omega \mathcal{W}(\Omega) = 0$). However, the central observable for the current analysis is the *signal-to-noise ratio* (SNR) of the wavelet transform, which we define as

$$\mathcal{S}(\Omega) \equiv \frac{\mathcal{F}_{\mathcal{W}}[\mathcal{C}](\Omega)}{\sqrt{\mathcal{F}_{\mathcal{W}^2}[\mathcal{C}](\Omega)}}, \quad (2)$$

where in the denominator the wavelet kernel is squared before performing the convolution. If the γ -ray flux varied only on scales much larger than the extent of the wavelet kernel, and in the limit of a large number of photons, $\mathcal{S}(\Omega)$ would behave like a smoothed Gaussian random field. *Consequently, $\mathcal{S}(\Omega)$ can be loosely interpreted as the local significance for having a source at position Ω , in units of standard deviations.*

As wavelet kernel, we adopt the second member of the Mexican Hat Wavelet Family, MHWF2, which was shown to provide very good source discrimination power [36], and which was used for identification of compact sources in Planck data [37]. The wavelet can be obtained by a successive application of the Laplacian operator to a two-dimensional Gaussian distribution with width $\sigma_b \cdot R$. Here, $\sigma_b = 0.4^\circ$ corresponds to the *Fermi*-LAT angular resolution at 1–4 GeV, and R is a tuning parameter. We find best results when R varies linearly with latitude

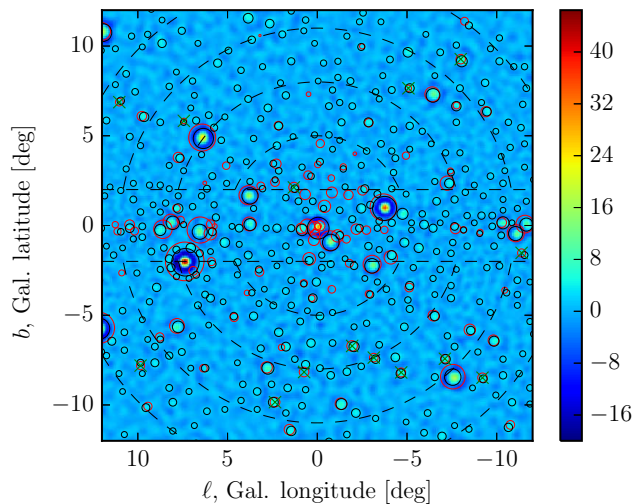


FIG. 1. SNR of the wavelet transform of γ -rays with energies in the range 1–4 GeV, $\mathcal{S}(\Omega)$. The black circles show the position of wavelet peaks with $\mathcal{S} \geq 2$; the red circles show the position of 3FGL sources. In both cases, the circle area scales with the significance of the source detection in that energy range. The dashed lines indicate the regions that we use for the binned likelihood analysis, where latitudes $|b| < 2^\circ$ are excluded because of the strong emission from the Galactic disk. The subset of 3FGL sources that remains unmasked in our analysis is indicated by the green crosses.

from $R = 0.53$ at $b = 0^\circ$ to $R = 0.83$ at $b = \pm 12^\circ$. This compensates to some degree the increasing diffuse backgrounds towards the Galactic disk, while optimizing the source sensitivity at higher latitudes [37].

The resulting SNR of the wavelet transform, $\mathcal{S}(\Omega)$, is shown in Fig. 1. As expected, the Galactic diffuse emission is almost completely filtered out by the wavelet transform, whereas bright sources lead to pronounced peaks. We adopt a simple algorithm for peak identification: We find all pixels in $\mathcal{S}(\Omega)$ with values larger than in the four adjacent pixels. We then clean these results from artefacts by forming clusters of peaks with coplanar distances less than 0.3° , and only keep the most significant peak in each cluster.

In Fig. 1, we show the identified wavelet peaks with peak significance $\mathcal{S} > 2$, as well as all 3FGL sources for comparison [1]. For sources that are bright enough in the adopted energy range, we find a good correspondence between wavelet peaks and the 3FGL, both in terms of position and significance (we compare the significance of wavelet peaks, \mathcal{S} , with the 1–3 GeV detection significance for 3FGL sources).

It is worth emphasizing that *for the adopted spherically symmetric and centrally peaked distribution of the CSP, most of the sources would be detected not directly at the GC, but a few degrees away from the Galactic disk.* This is simply due to the much weaker diffuse emission

at higher latitudes. Our focus on latitudes $|b| \geq 2^\circ$ thus avoids regions where source detection becomes less efficient, due to strong diffuse foregrounds, without significant sensitivity loss for the source population of interest.

3FGL sources. Before studying the statistics of the wavelet peaks in detail below, we remove almost all peaks that correspond to known 3FGL sources based on a 0.3° (1° for $\sqrt{TS} \geq 50$) proximity cut. However, in order to mitigate a potential bias on L_{\max} , we do not mask peaks that correspond to 3FGL sources that are likely part of the CSP. We identify such *MSP candidate sources* by requiring that they (i) are tagged as unassociated, (ii) show no indication for variability and (iii) have a spectrum compatible with MSPs. The last criterion is tested by performing a χ^2 -fit of the above MSP reference spectrum to the spectrum given in the 3FGL (0.1–100 GeV; five energy bins). Only the normalization is left free to vary. We require a fit quality of $\chi^2/\text{dof} \leq 1.22$ (with $\text{dof}=4$), corresponding to a p -value ≥ 0.3 .

We find 13 3FGL source in the inner Galaxy ROI that pass the above MSP cuts (listed in the supplementary material). Interestingly, the average number of MSP candidate sources in same-sized control regions along the Galactic disk in the range $|\ell| = 12^\circ\text{--}60^\circ$ is significantly smaller, with an average of 3.1. It is tempting to interpret this excess of MSP candidate sources in the inner Galaxy as being caused by the brightest sources of the CSP, above the less pronounced thick-disk population of MSPs [38]. However, we emphasize that the status of these 13 sources is currently neither clear, nor qualitatively decisive for our results. Whether we mask them plays a minor role for the detection of the CSP below (but does affect the inferred values for L_{\max} , see supplementary material).

Statistical analysis. In Fig. 2 we show a histogram of the wavelet peaks in our ROI. We bin the peaks in a two-dimensional grid, which spans the projected Galactocentric angle $2^\circ\text{--}17^\circ$, and wavelet peak significances in the range 1–10. The bin edges are as indicated in the figure. As expected, photon shot noise gives rise to a large number of peaks with low significances $\mathcal{S} \leq 3$, and only a small number of peaks has $\mathcal{S} \geq 5$.

We assume that the number of peaks in each bin in Fig. 2 follows – in repeated experiments and random realizations of the CSP – to a good approximation a Poisson distribution. We estimate the corresponding average number of expected wavelet peaks in each bin using a large number of Monte Carlo (MC) simulations, where we simulate the diffuse background emission, random realizations of the source population and photon shot noise.

In order to quantify what CSP luminosity function reproduces best the observations, we perform a binned Poisson likelihood analysis of the wavelet peak distribu-

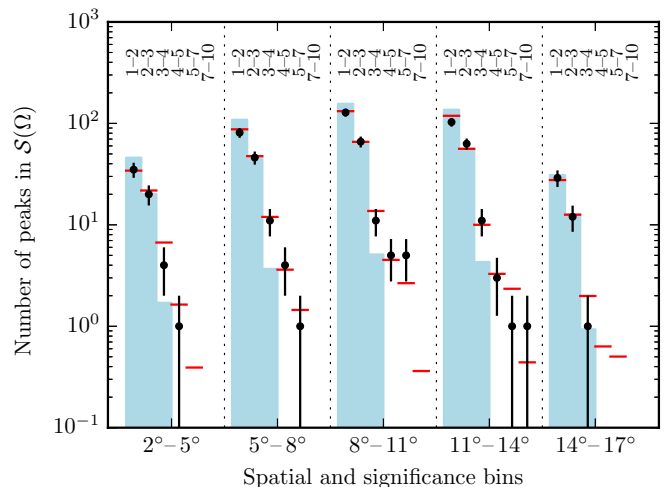


FIG. 2. Histogram of observed peaks in $\mathcal{S}(\Omega)$, in bins of projected radial distance from the GC and SNR values (black dots with statistical error bars). We show the expectation value for the case of a negligible CSP as blue bars, whereas the expectation values for the best-fit are shown in red.

tion. The likelihood function is given by

$$\mathcal{L} = \prod_{i=1}^{n_r} \prod_{j=1}^{n_s} \mathcal{P}(c_{ij} | \mu_{ij}(L_{\max}, \Phi_5)), \quad (3)$$

where n_r and n_s are respectively the numbers of radial and peak SNR bins, c_{ij} are the observed and μ_{ij} the expected number of peaks, and \mathcal{P} is a Poisson distribution. The expectation values depend directly on the maximal luminosity, L_{\max} , as well as on the number of simulated sources, n . To ease comparison with the literature, we determine n as a function of Φ_5 , which denotes the mean differential intensity of the CSP at $b = \pm 5^\circ$, $\ell = 0^\circ$ and 2 GeV. In the case of the GCE, this value was found to be $\Phi_5^{\text{GCE}} = (8.5 \pm 1.5) \times 10^{-7} \text{ GeV}^{-1} \text{ cm}^{-2} \text{ s}^{-1} \text{ sr}^{-1}$ at 95.4% CL [15].

Results. In Fig. 2, we show the expectation values that we obtain when neglecting contributions from the CSP (and any other non-diffuse emission). This corresponds to good approximation to the case where the GCE is of truly diffuse origin, including the case of DM annihilation or outburst events. We find that the observed number of wavelet peaks with $\mathcal{S} < 2$ is significantly lower than expected, whereas the observed number of peaks with $\mathcal{S} > 3$ is significantly higher. As we will show next, *this is precisely the effect that is caused by a dim source population.*

We now turn to the case with a non-zero CSP contribution. In Fig. 3, we show the limits that we obtain on the two CSP parameters when fitting the histogram in Fig. 2 as described above. We find that a non-zero contribution

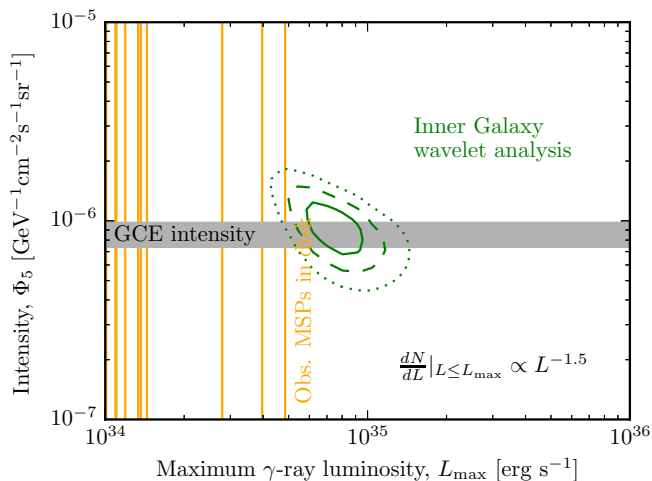


FIG. 3. Constraints on the maximum γ -ray luminosity of the CSP, L_{\max} , and the population averaged intensity at $b = \pm 5^\circ$, $\ell = 0^\circ$ and 2 GeV, Φ_5 , as derived from our wavelet analysis. We show 68.7%, 95.4% and 99.7% CL contours. We also indicate the values of Φ_5 where the source population can explain 100% of the GCE (horizontal gray band, 95.4% CL), and as vertical orange lines the luminosity of the brightest observed nearby MSPs.

from the CSP is favoured at the level of at least 10.8σ .² The best-fit value for the total differential intensity is $\Phi_5 = (9.0 \pm 1.9) \times 10^{-7} \text{ GeV}^{-1} \text{ cm}^{-2} \text{ s}^{-1} \text{ sr}^{-1}$ and for the maximum luminosity $L_{\max} = (7.5 \pm 1.4) \times 10^{34} \text{ erg s}^{-1}$. As can be seen in Fig. 2, we obtain in this case a very good fit to the data.

Our preferred range of the maximum γ -ray luminosities reaches up to $L_{\max} \leq 1.04 \times 10^{35} \text{ erg s}^{-1}$ (at 95.4% CL), which is compatible with observations of nearby MSPs. We illustrate this by showing in Fig. 3 the γ -ray luminosity of the brightest individually observed nearby MSPs as given in Ref. [35].³ Furthermore, for the adopted slope of the luminosity function, $\alpha = 1.5$, the best-fit value for the total differential intensity of the CSP, Φ_5 , is consistent with the CSP accounting for 100% of the GCE emission.

Discussion and conclusions. We found corroborating evidence for the hypothesis that the GCE is caused by a hitherto undetected population of MSP-like sources. We performed a wavelet transform of the γ -ray emission from the inner Galaxy, which removes Galactic diffuse emission and enhances point sources, and we studied the

statistics of the peaks in this transform. We detected with 10.8σ significance a suppression (enhancement) of low (high)-significance wavelet peaks, relative to the expectations for purely diffuse emission. We showed that this effect is caused by the presence of a large number of dim point sources. The spatial distribution of wavelet peaks in the inner Galaxy is compatible with a centrally peaked source distribution, and the inferred cutoff of the γ -ray luminosity function of these sources agrees with the observation of nearby MSPs. This source population can, for reasonable slopes of the luminosity function, account for 100% of the GCE emission.

For the purpose of this *Letter*, which introduces a new method, we kept our analysis as simple as possible. In general, our results could be affected by the presence of extragalactic and Galactic sources, by the thick-disk population of MSPs and young pulsars, by the details of masking and unmasking 3FGL sources, by the details of the adopted γ -ray luminosity function, and by substructures in the Galactic diffuse emission that are not removed by the wavelet transform. We address all of these points in the supplementary material and show that it is unlikely that they affect our results qualitatively, although quantitative changes in the obtained best-fit values for Φ_5 and L_{\max} are possible. A much more detailed analysis will be presented in a future publication.

The prospects for fully establishing the MSP interpretation within the coming decade are very good. Our results suggest that upcoming γ -ray observations with improved angular resolution (planned/proposed γ -ray satellites like GAMMA-400 [39], ASTROGAM and PANGU [40]) will allow to detect many more of the bulge sources, and to study their distribution and spectra. For current radio instruments, it remains rather challenging to detect a MSP population in the bulge [25], but prospects for next-generation instruments are good.

Acknowledgments. We thank for useful discussions with David Berge, Francesca Calore, Ilias Cholis, Jennifer Gaskins, Dan Hooper, Simona Murgia, Tracy Slatyer, Ben Safdi and Jacco Vink. We thank the *Fermi* collaboration for providing the public *Fermi* data as well as the *Fermi* Science Tools (v10r0p5). SURFsara is thanked for use of the Lisa Compute Cluster. SK and CW (P.I.) are part of the VIDI research programme “Probing the Genesis of Dark Matter”, which is financed by the Netherlands Organisation for Scientific Research (NWO). RB is part of a GRAPPA-PhD program funded by NWO. Part of this work was performed at the Aspen Center for Physics, which is supported by National Science Foundation grant PHY-1066293.

Note added. While finalizing our work, we became aware of another group studying dim γ -ray sources in the inner Galaxy, using non-Poissonian photon statistics [41].

² When quoting the statistical significance, we conservatively take into account bins with $S < 5$ only, which are most affected by a dim source population, and least affected by the masking of 3FGL sources (see supplementary material for details).

³ We only show objects where 2PC [32] distances are available; see Ref. [25] for a detailed discussion about distance uncertainties.

-
- * r.t.bartels@uva.nl
† s.krishnamurthy@uva.nl
‡ c.weniger@uva.nl
- [1] The Fermi-LAT Collaboration, ArXiv e-prints (2015), arXiv:1501.02003 [astro-ph.HE].
- [2] M. Su, T. R. Slatyer, and D. P. Finkbeiner, *Astrophys. J.* **724**, 1044 (2010), arXiv:1005.5480 [astro-ph.HE].
- [3] M. Ackermann *et al.* (Fermi-LAT), (2015), arXiv:1503.02641 [astro-ph.HE].
- [4] J.-Q. Xia, A. Cuoco, E. Branchini, and M. Viel, *Astrophys.J.Suppl.* **217**, 15 (2015), arXiv:1503.05918 [astro-ph.CO].
- [5] L. Goodenough and D. Hooper, (2009), arXiv:0910.2998 [hep-ph].
- [6] V. Vitale and A. Morselli (Fermi/LAT Collaboration), (2009), arXiv:0912.3828 [astro-ph.HE].
- [7] D. Hooper and L. Goodenough, *Phys.Lett.* **B697**, 412 (2011), arXiv:1010.2752 [hep-ph].
- [8] D. Hooper and T. Linden, *Phys.Rev.* **D84**, 123005 (2011), arXiv:1110.0006 [astro-ph.HE].
- [9] K. N. Abazajian and M. Kaplinghat, *Phys.Rev.* **D86**, 083511 (2012), arXiv:1207.6047 [astro-ph.HE].
- [10] C. Gordon and O. Macias, *Phys.Rev.* **D88**, 083521 (2013), arXiv:1306.5725 [astro-ph.HE].
- [11] O. Macias and C. Gordon, *Phys.Rev.* **D89**, 063515 (2014), arXiv:1312.6671 [astro-ph.HE].
- [12] K. N. Abazajian, N. Canac, S. Horiuchi, and M. Kaplinghat, *Phys.Rev.* **D90**, 023526 (2014), arXiv:1402.4090 [astro-ph.HE].
- [13] T. Daylan, D. P. Finkbeiner, D. Hooper, T. Linden, S. K. N. Portillo, *et al.*, (2014), arXiv:1402.6703 [astro-ph.HE].
- [14] B. Zhou, Y.-F. Liang, X. Huang, X. Li, Y.-Z. Fan, *et al.*, (2014), arXiv:1406.6948 [astro-ph.HE].
- [15] F. Calore, I. Cholis, and C. Weniger, *JCAP* **1503**, 038 (2015), arXiv:1409.0042 [astro-ph.CO].
- [16] S. Murgia, “Observation of the high energy gamma-ray emission towards the Galactic center,” (2014), Talk given on Fifth Fermi Symposium, Nagoya, 20-24 October 2014.
- [17] D. Hooper and T. R. Slatyer, *Phys.Dark Univ.* **2**, 118 (2013), arXiv:1302.6589 [astro-ph.HE].
- [18] W.-C. Huang, A. Urbano, and W. Xue, (2013), arXiv:1307.6862 [hep-ph].
- [19] E. Carlson and S. Profumo, *Phys.Rev.* **D90**, 023015 (2014), arXiv:1405.7685 [astro-ph.HE].
- [20] J. Petrovic, P. D. Serpico, and G. Zaharijas, *JCAP* **1410**, 052 (2014), arXiv:1405.7928 [astro-ph.HE].
- [21] I. Cholis, C. Evoli, F. Calore, T. Linden, C. Weniger, and D. Hooper, (2015), arXiv:1506.05119 [astro-ph.HE].
- [22] D. Gaggero, M. Taoso, A. Urbano, M. Valli, and P. Ullio, (2015), arXiv:1507.06129 [astro-ph.HE].
- [23] K. N. Abazajian, *JCAP* **1103**, 010 (2011), arXiv:1011.4275 [astro-ph.HE].
- [24] Q. Yuan and B. Zhang, *JHEAp* **3-4**, 1 (2014), arXiv:1404.2318 [astro-ph.HE].
- [25] T. D. Brandt and B. Kocsis, (2015), arXiv:1507.05616 [astro-ph.HE].
- [26] R. Voss and M. Gilfanov, *Astron. and Astroph.* **468**, 49 (2007), astro-ph/0610649.
- [27] K. N. Abazajian and M. Kaplinghat, *Phys. Rev. D* **86**, 083511 (2012), arXiv:1207.6047 [astro-ph.HE].
- [28] K. Perez, C. J. Hailey, F. E. Bauer, R. A. Krivonos, K. Mori, F. K. Baganoff, N. M. Barrière, S. E. Boggs, F. E. Christensen, W. W. Craig, B. W. Grefenstette, J. E. Grindlay, F. A. Harrison, J. Hong, K. K. Madsen, M. Nynka, D. Stern, J. A. Tomsick, D. R. Wik, S. Zhang, W. W. Zhang, and A. Zoglauer, *Nature (London)* **520**, 646 (2015).
- [29] D. Hooper, I. Cholis, T. Linden, J. Siegal-Gaskins, and T. Slatyer, *Phys.Rev.* **D88**, 083009 (2013), arXiv:1305.0830 [astro-ph.HE].
- [30] I. Cholis, D. Hooper, and T. Linden, (2014), arXiv:1407.5625 [astro-ph.HE].
- [31] J. Petrovi, P. D. Serpico, and G. Zaharijas, *JCAP* **1502**, 023 (2015), arXiv:1411.2980 [astro-ph.HE].
- [32] A. Abdo *et al.* (The Fermi-LAT collaboration), *Astrophys.J.Suppl.* **208**, 17 (2013), arXiv:1305.4385 [astro-ph.HE].
- [33] *Astrophys. J. Suppl.* **199**, 31 (2012), arXiv:1108.1435 [astro-ph.HE].
- [34] S. K. Lee, M. Lisanti, and B. R. Safdi, *JCAP* **1505**, 056 (2015), arXiv:1412.6099 [astro-ph.CO].
- [35] I. Cholis, D. Hooper, and T. Linden, (2014), arXiv:1407.5583 [astro-ph.HE].
- [36] J. Gonzalez-Nuevo, F. Argueso, M. Lopez-Caniego, L. Toffolatti, J. Sanz, *et al.*, *Mon.Not.Roy.Astron.Soc.* **369**, 1603 (2006), arXiv:astro-ph/0604376 [astro-ph].
- [37] P. Ade *et al.* (Planck), *Astron.Astrophys.* **571**, A28 (2014), arXiv:1303.5088 [astro-ph.CO].
- [38] F. Calore, M. Di Mauro, F. Donato, and F. Donato, *Astrophys.J.* **796**, 1 (2014), arXiv:1406.2706 [astro-ph.HE].
- [39] N. Topchiev, A. Galper, V. Bonvicini, O. Adriani, R. Aptekar, *et al.*, *Bull.Russ.Acad.Sci.Phys.* **79**, 417 (2015).
- [40] X. Wu, M. Su, A. Bravar, J. Chang, Y. Fan, *et al.*, *Proc.SPIE Int.Soc.Opt.Eng.* **9144**, 91440F (2014), arXiv:1407.0710 [astro-ph.IM].
- [41] S. K. Lee, M. Lisanti, B. R. Safdi, T. R. Slatyer, and W. Xue, (2015), arXiv:1506.05124 [astro-ph.HE].
- [42] A. W. Strong, *Astrophys.Space Sci.* **309**, 35 (2007), arXiv:astro-ph/0609359 [astro-ph].
- [43] C. Venter, T. Johnson, A. Harding, and J. Grove, (2014), arXiv:1411.0559 [astro-ph.HE].
- [44] J.-M. Casandjian, *Astrophys. J.* **806**, 240 (2015), arXiv:1506.00047 [astro-ph.HE].
- [45] T. Dame, D. Hartmann, and P. Thaddeus, *Astrophys.J.* **547**, 792 (2001), arXiv:astro-ph/0009217 [astro-ph].

SUPPLEMENTARY MATERIAL

In the supplementary material, we discuss the possible impact of various systematic effects on our results. This includes a control region analysis, a discussion of various types of gamma-ray sources, substructure in diffuse emission, and a thick-disk population of MSPs.

A. Null results in control regions

In order to estimate the effect of various systematic uncertainties, it is useful to apply our analysis on control regions along the Galactic disk (in the case of Galactic diffuse emission this was first systematically done in Ref. [15]). Potentially unresolved substructure in the Galactic diffuse emission (e.g. in the form of giant molecular clouds, see below), and contributions from various Galactic and extragalactic source populations could be responsible for the detected wavelet signal in the inner Galaxy, but would in general also affect other regions in the Galactic disk. To this end, we focus on (partially overlapping) control regions along the Galactic disk, which are of the same size as the inner Galaxy ROI, but displaced by $\Delta\ell = \pm k 20^\circ$ with $k = 1, 2, 3, 4$.

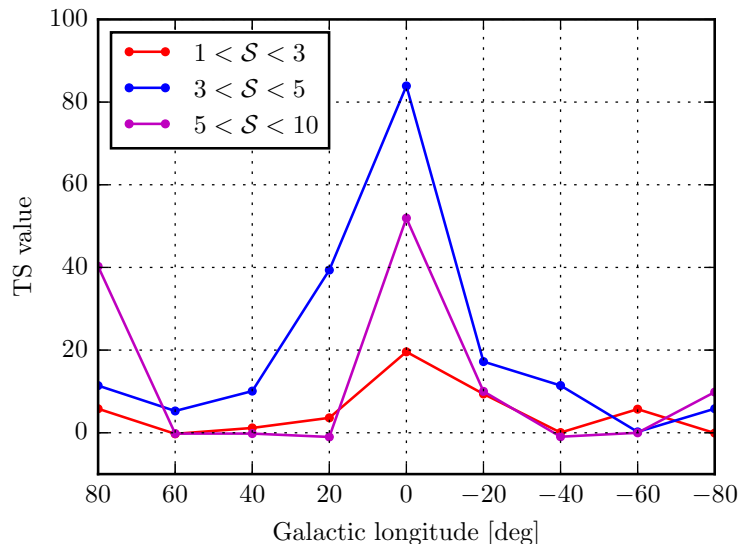


FIG. S-4. We show, as function of the central longitudinal position of the control regions (for $\ell = 0^\circ$ the main ROI), the significance of a CSP detection. We assume that the CSP is centered in each of the ROIs, and we refit the parameters L_{\max} and the number of sources. We indicate how different ranges of the wavelet peak significances contribute to the detection. *All* 3FGL sources are masked in this plot, in order to be conservative.

In Fig. S-4 we show the TS value for a detection of the CSP for the main and the different control ROIs along the Galactic disk. We leave L_{\max} and Φ_5 free to vary in each region independently. In the main ROI that covers the inner Galaxy we find the significant detection of a CSP that was discussed in the main text. As shown in the plot, this high significance is supported by the low, intermediate and high-significance SNR peaks of the wavelet transform separately. The directly adjacent regions also show relatively large TS values, which is either caused by the partial overlap of these control regions with the main ROI, or by a CSP that is more disk-like than assumed in our analysis. We will address the latter point below. However, in the outermost six control regions we find no significant detection of a CSP, for any of the considered values for L_{\max} and Φ_5 (the large TS values at $\ell = 80^\circ$ are caused by one extremely bright source that generates fake peaks in its tails). This observation makes it already extremely unlikely that our findings are driven by a mismodelling of the local Galactic diffuse emission, or by extragalactic sources. We will address this in more detail below.

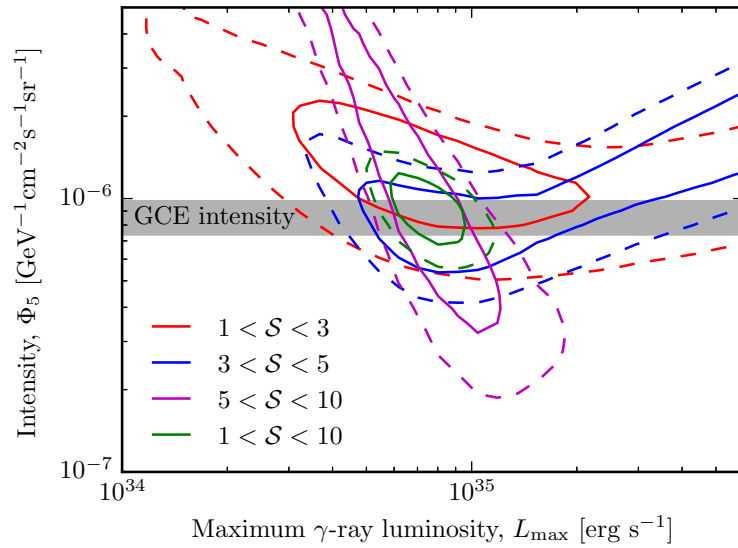


FIG. S-5. Similar to Fig. 3 in the main text, but showing limits derived for different ranges of the wavelet peak significances separately. The parameter degeneracies present in some of the fits cancel when fitting the entire significance range at once. We only show 68.7% and 95.4% CL constraints for clarity.

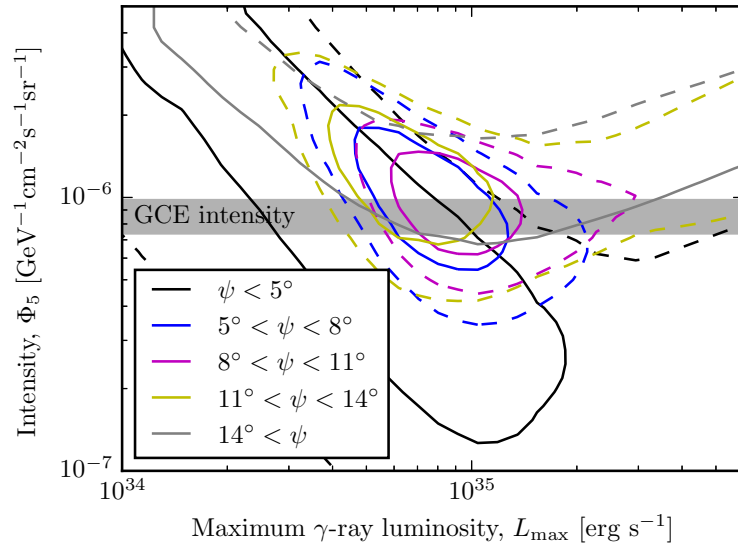


FIG. S-6. Similar to Fig. 3 in the main text, but showing limits as derived for different spatial bins separately.

B. Consistent wavelet signal in separate bins

It is instructive to see how wavelet peaks with different significances contribute to the constraints on the luminosity function that we showed in Fig. 3 in the main text. To this end, we show in Fig. S-5 the limits that we obtain separately from peak significances in the range $\mathcal{S} = 1-3$, $\mathcal{S} = 3-5$ and $\mathcal{S} = 5-10$, respectively. All three constraints are mutually consistent to within 1σ , leading to a consistent interpretation of the peaks shown in Fig. 1 in the main text. In all cases we find some degeneracy in the (L_{\max}, Φ_5) plane. High significance peaks predominantly provide a stringent upper limit on L_{\max} , whereas low significance peaks mostly constrain the overall luminosity of the modeled source population.

To show that our assumption on the spatial distribution of the CSP is consistent with the data, we show Fig. S-6

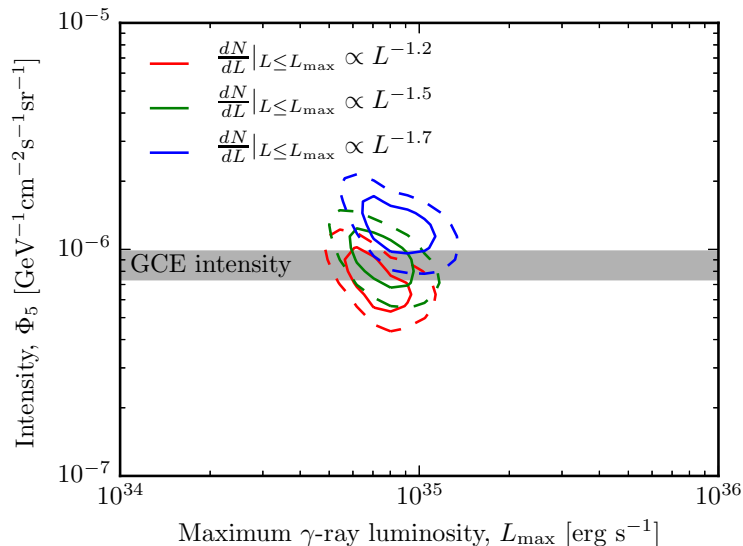


FIG. S-7. Similar to Fig. 3 in the main text. We show the 68.7% and 95.4% CL contours for luminosity functions with spectral indices of 1.2, 1.5 and 1.7.

the result obtained for the five different spatial bins independently. Ring 1–5 correspond to $r \in [i^\circ, i + 3^\circ]$ with $i = 2, 5, 8, 11, 14$, respectively. We find constraints on L_{\max} and Φ_5 that are consistent to within 1σ .

Finally, we checked that the identified wavelet peaks are symmetrically distributed in the north, south, east and west parts of our main ROI. Only at $S > 3$ we find a slight (statistically not very significant) asymmetry with more peaks in the south, which might be caused by the somewhat stronger Galactic foregrounds in the north, which makes point source detection in the north more challenging.

C. Mild dependence on the MSP luminosity function

Theoretically α is not well constrained and can plausibly range from 1.5 to 3, depending on the emission model [31, 42, 43]. Actual MSP observations actually seem to indicate somewhat smaller values closer to $\alpha \sim 1.2$ [35]. We show in Fig. S-7 the 68.7% and 95.4% CL contours for different luminosity functions, respectively with spectral indices of 1.2 and 1.7. For a fixed intensity (Φ_5), hardening (softening) of the luminosity function corresponds to an enhancement (suppression) of the number of sub-threshold point sources, which explains the direction in which the best fit region moves. We note that we obtain very similar TS values for all slopes that we considered.

D. The role of unmasked 3FGL sources

In the present analysis, we make use of the 3FGL, the third *Fermi* source catalogue, which is based on the first four years of *Fermi* pass 7 data. One important ingredient in our analysis is the masking of 3FGL sources. These sources are of Galactic and extragalactic origin and leaving them unmasked would inevitably induce sizeable signals in our search for a sub-threshold source population in the bulge. However, as discussed in the main text, we keep unassociated sources with MSP-like spectra unmasked. These sources could be part of the bulge MSP population that we are looking for, and masking them would bias our results. The 13 sources that pass our MSP cuts are listed in Tab. I.

In general, falsely masking unassociated sources that actually belong to the bulge MSP population would push L_{\max} to lower values, whereas falsely unmasking foreground sources would push it to large values. This is illustrated in Fig. S-8. We show the case where we mask *all* unassociated sources, as well as the case where we adopt a weaker criterion for the spectral fit, leaving around 20 sources unmasked. We find that in both cases the best-fit value for L_{\max} moves in the expected direction, but the results remain consistent to within 1σ . Furthermore, the significance of our wavelet detection that we quote in the main text (where we include $\mathcal{S} < 5$ bins only) changes to 9.9σ when we

3FGL Name	ℓ [°]	b [°]	χ^2/dof	\sqrt{TS}	\mathcal{S}	$L[10^{34} \text{ erg/s}]$
J1649.6-3007	-7.99	9.27	1.07	5.6	7.4	$7.8^{+5.5}_{-2.7}$
J1703.6-2850	-5.08	7.65	0.48	2.4	5.0	$3.4^{+2.4}_{-1.2}$
J1740.5-2642	1.30	2.12	0.37	6.4	3.5	$14.9^{+10.6}_{-5.1}$
J1740.8-1933	7.43	5.83	0.77	1.9	2.3	$3.8^{+2.7}_{-1.3}$
J1744.8-1557	11.03	6.88	0.40	3.7	3.4	$5.6^{+3.9}_{-1.9}$
J1758.8-4108	-9.21	-8.48	0.90	5.6	3.8	$4.8^{+3.4}_{-1.7}$
J1759.2-3848	-7.11	-7.43	0.35	4.6	5.6	$5.9^{+4.2}_{-2.0}$
J1808.3-3357	-1.94	-6.71	0.40	6.9	6.3	$8.0^{+5.7}_{-2.7}$
J1808.4-3519	-3.15	-7.36	0.41	4.6	4.4	$5.0^{+3.5}_{-1.7}$
J1808.4-3703	-4.68	-8.19	0.22	4.9	5.3	$4.3^{+3.1}_{-1.5}$
J1820.4-3217	0.74	-8.17	1.04	5.7	1.7	$7.2^{+5.1}_{-2.5}$
J1830.8-3136	2.35	-9.84	0.54	5.9	6.0	$5.0^{+3.6}_{-1.7}$
J1837.3-2403	9.85	-7.81	0.28	4.0	3.0	$4.7^{+3.3}_{-1.6}$

TABLE I. List of the 13 unassociated 3FGL sources with MSP-like spectra, which we leave unmasked in our analysis. It is likely that some or most of them are part of the CSP. The last four columns show the goodness-of-fit of the reference MSP spectrum, the 3FGL significance in the 1–3 GeV band, the corresponding peak of the wavelet SNR, and the γ -ray luminosity assuming 8.5 ± 2 kpc distance from the source.

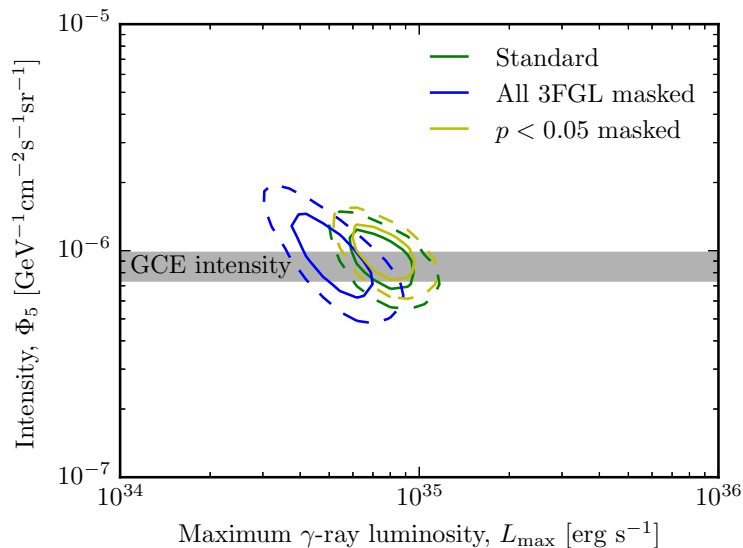


FIG. S-8. Similar to Fig. 3 in the main text. We show the effect of masking *all* 3FGL sources, or leaving a slightly larger number unmasked.

mask all sources, and to 11.9σ when keeping 20 sources unmasked. The (un-)masking of 3FGL is hence not decisive for our qualitative findings, although quantitative results can be affected.

It is interesting to note that the faintest 3FGL source in the inner Galaxy ROI that passes our MSP-spectrum cut, has a luminosity of $L = 3.4 \times 10^{34} \text{ erg s}^{-1}$ if placed at 8.5 kpc distance. This is a good, though rough, indication for the *de facto* sensitivity threshold of *Fermi*-LAT for the detection of sources with MSP-like spectra in the bulge region.

Lastly, one can use the sources in Tab. I to compare the sensitivity of the 3FGL with our wavelet analysis. Averaging over the 13 sources, we find a ratio of $\mathcal{S}/\sqrt{TS} \simeq 1.0 \pm 0.4$, indicating that the sensitivity of the wavelet method is similar to the 3FGL sensitivity in a comparable energy range. However, the scatter exceeds the one expected from statistical fluctuations alone, which can be attributed to differences in the systematics that affect the 3FGL and the wavelet analysis.

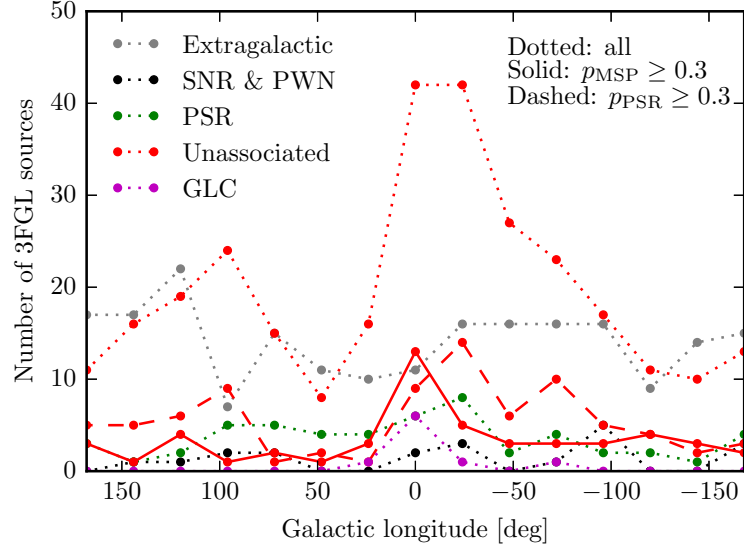


FIG. S-9. Latitude profile of sources, for different ROIs along the Galactic disk, as function of their longitudinal center (dotted lines). The ROIs have a size of $24^\circ \times 24^\circ$, with the Galactic disk, $|b| < 2^\circ$, masked. The different colors correspond to different source categories. In the case of unassociated sources, the solid (dashed) lines show only sources that pass the spectrum cut for MSP-like (young pulsar-like) sources.

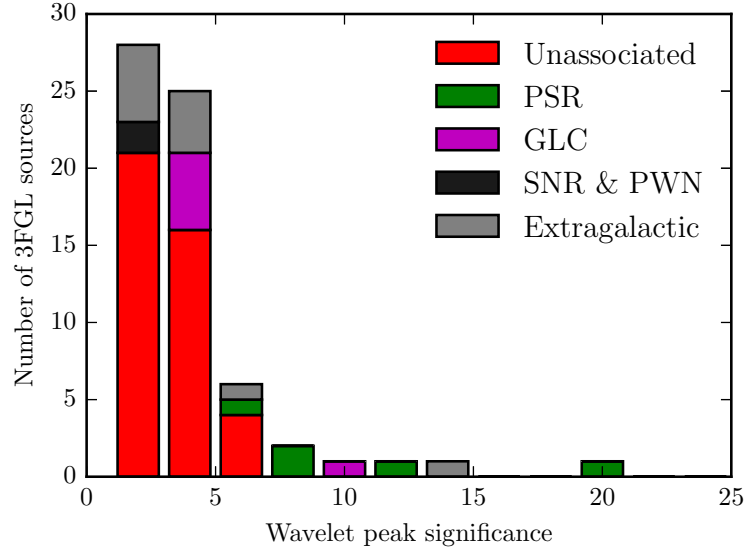


FIG. S-10. Stacked histogram of wavelet peak values \mathcal{S} that correspond to 3FGL sources in the inner Galaxy ROI. We show the contribution from different source categories separately. Unassociated sources generate mostly low-significance wavelet peaks, whereas for example source that are marked as pulsar in the 3FGL only generate peaks with a high significance (see discussion).

E. The role of various source populations

In Fig. S-9, we show the number of 3FGL sources in our inner Galaxy ROI as well as in various same-sized ROIs that are displaced along the Galactic disk in steps of $\Delta\ell = \pm 24^\circ$. We show (identified and associated) extragalactic sources, various Galactic source classes and unassociated sources classes separately. We also show for all source categories how many sources pass our MSP cut. It is apparent that the number of unassociated sources strongly peaks in the inner Galaxy ROI, however with a clear asymmetry towards negative values of ℓ , and another peak around $\ell \approx 100^\circ$. However, after applying the MSP cut, predominantly sources in the inner Galaxy survive. In Fig. S-10, on the other

hand, we show a histogram of the wavelet peak significance that our analysis attributes to the 3FGL sources in the inner Galaxy ROI. Again, unassociated sources play a major role and produce wavelet peaks down to values of $\mathcal{S} \sim 1$. On the other hand, 3FGL sources that are identified as pulsars appear only with $\mathcal{S} > 5$ in our analysis. We will discuss in the following the potential impact of each of the source classes separately.

Extragalactic sources. As shown in Fig. S-9, the number of extragalactic sources in the individual ROIs along the Galactic disk fluctuates around values of about ~ 13 . No significant suppression is observed in the inner Galaxy ROI, which would have indicated that it is more challenging to identify or associate extragalactic sources in this region. We will use here a simple argument to show that extragalactic sources cannot play a significant role for our results. The average number of $\mathcal{S} = 3-5$ wavelet peaks in the above control regions along the Galactic disk is 20; in the inner Galaxy ROI it is 42 (we exclude here *all* 3FGL sources to be conservative). If extragalactic sources were the main contribution to these peaks, in addition to the about 10 wavelet peaks that are expected from statistical fluctuations alone (see Fig. 2 in the main text), the 42 observed peaks would constitute a $> 5\sigma$ upward fluctuation above the expected 20. This makes it extremely unlikely that extragalactic sources contribute significantly to our results in the inner Galaxy. Similar arguments can be made using wavelet peaks in the range $\mathcal{S} = 1-2$.

Supernova remnants and pulsar wind nebulae. As apparent in Fig. S-9, only a very small number of sources along the Galactic disk at latitudes $|b| > 2^\circ$ (and almost none at $|b| > 5^\circ$) are identified with supernova remnants or pulsar wind nebulae. In our ROIs their number is much less than the number of extragalactic sources, and their distribution is centrally not peaked, indicating that sources at these latitudes are mostly local. Sources in this category are typically more easily detectable at higher and lower energies than the energy range used in our analysis, and would be most likely listed in the 3FGL and hence masked if they were abundant and significant. We consider it hence as extremely unlikely that sources of this category significantly affect our results in the inner Galaxy.

Young and millisecond pulsars. An interesting feature of pulsars in the 3FGL is that they always induce large wavelet signals in our analysis, as shown in Fig. S-10. This makes indeed sense, since the identification of a γ -ray source as pulsar requires the measurement of its pulsation, and hence a large enough number of photons. Furthermore, the pulsar energy spectrum often peaks close the energy range of our analysis. Already from Fig. S-10 it is obvious that a large fraction of the unassociated sources, which mostly appear with lower significance peaks, must in fact be pulsars. Interestingly, as shown in Fig. S-9, identified pulsars do not show a centrally peaked distribution, whereas the unassociated sources clearly do. This behaviour is expected, given that with increasing distance the pulsar identification becomes more challenging.

Globular clusters. The γ -ray emission from globular clusters that is not masked in our analysis, either because the globular clusters did not enter the 3FGL, or because they happen to be among our 13 unmasked unassociated sources, could in principle contribute to the detected signal. Since their total emission is usually due to several MSPs which appear as a single source for *Fermi*-LAT, their presence could bias L_{\max} towards larger values. However, given the simulation results from Ref. [25], we expect this effect to be small, and leave a more detailed discussion to future work.

Unassociated sources. The peak of unassociated sources in the inner Galaxy, as shown in Fig. S-9, appears clearly asymmetric, with a second peak at $\ell \approx 100^\circ$. As discussed above, a large fraction of these sources is expected to be young or millisecond pulsars. Obviously, the 3FGL unassociated sources do not directly contribute to our results since they are masked (except the 13 MSP candidates). However, the unassociated sources are extremely abundant even down to $\mathcal{S} \sim 1$, and their probable nature can be used as an indicator for what source population dominates just below threshold.

In Fig. S-9, we see that our MSP cut removes most of the unassociated sources, but leaves an excess of 13 unassociated sources in the inner Galaxy, as discussed above. What is more, if we slightly modify the spectral criterion, using $dN/dE \propto e^{-E/2 \text{ GeV}} E^{-2}$, which is somewhat more pulsar-like (softer index, lower cutoff), this behaviour changes and we instead find excesses that are more correlated with the peaks of the unassociated sources away from the inner Galaxy. Although the statistical significance of this finding is rather difficult to quantify without a detailed study (which we leave for future work), this result is indicative. It suggests that a large fraction of the inner Galaxy unassociated (and sub-threshold) sources are likely MSPs, whereas unassociated sources in other parts of the disk have a larger fraction of young pulsars. The latter point is further supported by the fact that similar structures can be found in the longitudinal distribution of identified pulsars.

In summary, we expect that our wavelet signal is dominated by whatever source class is responsible for most of the unassociated sources towards the inner Galaxy. Very likely, these are millisecond and young pulsars, with a somewhat higher MSP/young pulsar ratio than in the rest of the disk. Since these sources appear in general both in the Galactic disk as well as in the bulge, it is important to study whether the excess/suppression of wavelet peaks in the inner Galaxy points to a disk population, a bulge population, or to a combination of both. This will be discussed in the

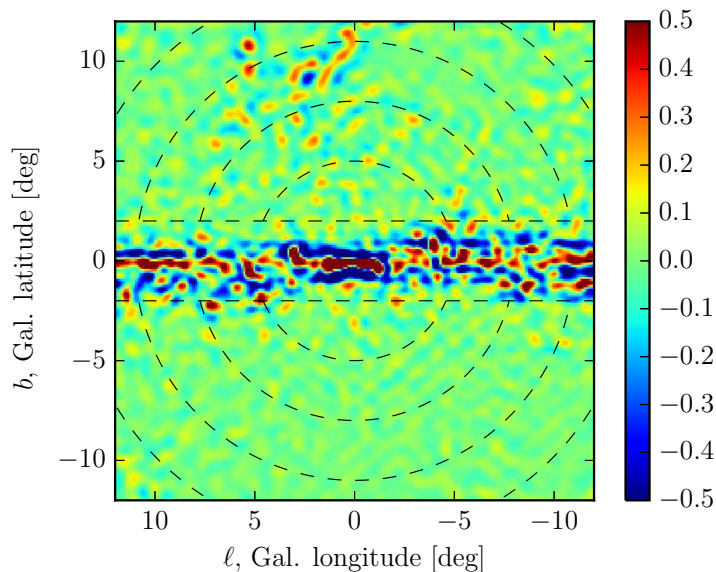


FIG. S-11. Similar to Fig. 1 in the main text (note the different color scale), but showing the transform of the diffuse BG model only, without Poisson noise being applied. Outside of the Galactic disk, $|b| > 2^\circ$, which we exclude from our analysis, the significance of wavelet peaks remains below 0.5. The variance is below 0.1, which shows that even 1σ peaks in the wavelet transform are unlikely to be strongly affected by the Galactic diffuse emission.

last subsection.

F. Caveats concerning the Galactic diffuse emission

In our Monte Carlo studies, we use the standard *Fermi* diffuse model for pass 8 data analysis. The wavelet transform of this model, *without applying Poisson noise*, but using the same exposure as in our main analysis, is shown in Fig. S-11. Outside of the masked Galactic disk at $|b| > 2^\circ$, we do not find any excesses with a significance larger than about 0.5σ . The main effect of such variations would be to offset the significance of random statistical fluctuations and sub-threshold point sources towards higher or lower values. This would not significantly affect peaks with a large SNR. However, it can potentially be important for low-significance peaks, because the collective shift of a large number of peaks, even by a small amount, could become statistically relevant. However, since the variance of the SNR values shown in Fig. S-11 is below 0.1, we do not expect that the details of the modeling of diffuse emission when doing MCs is going to affect our results.

However, the *Fermi* diffuse models might not actually contain all small-scale gas structures. Assuming a typical differential gamma-ray emissivity (at 1 GeV) of $\sim 3 \times 10^{-26} \text{ s}^{-1} \text{ GeV}^{-1}$ per hydrogen atom [44], we find that a giant molecular cloud with a mass of about $3 \times 10^5 M_\odot$ would be, at 1 GeV, roughly as bright as a MSP with $L = 7 \times 10^{34} \text{ erg s}^{-1}$ (we note for reference that for such a MSP, placed at the GC, we would have seen around 270 photons in our energy range). Our non-detection along the Galactic disk in Fig. S-4 suggest that mismodeling of *local* gas is unlikely the cause for the detected signal towards the inner Galaxy, since it should affect other parts of the disk as well. However, a large number of clouds of similar size, distributed in the Galactic bulge up to high latitudes, could in principle give rise to the observed signal. Although there is no observational evidence for the existence of such clouds (which should give rise to signals in the $\mathcal{O}(10\text{--}100) \text{ K km s}^{-1}$ range in CO observations [45]), we currently cannot rule out this interpretation.

G. Potential impact of thick-disk population

We finally show that it is rather unlikely that a thick-disk population of sources can account for a dominant part of the CSP detection in the inner Galaxy. As argued above, we expect that the most relevant Galactic background in our ROI are pulsars, and in particular the MSP thick-disk population that reaches up to high latitudes. We perform MC

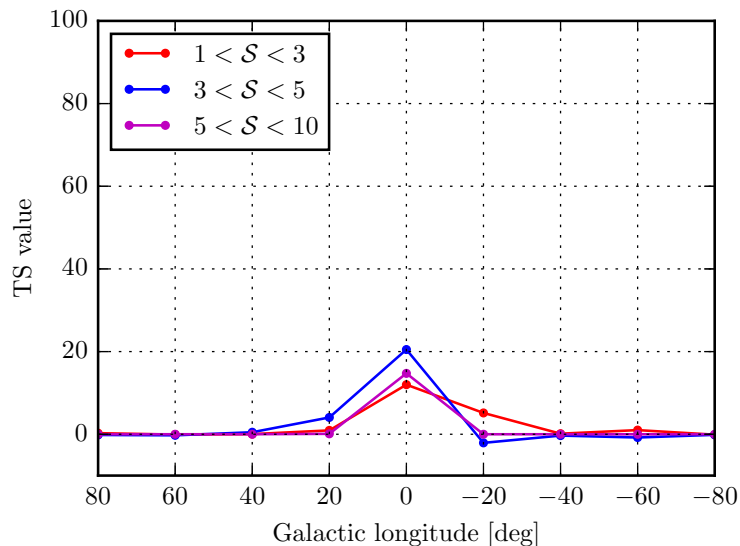


FIG. S-12. Similar to Fig. S-4, but including an extreme thick-disk MSP population as additional background that is tuned to absorb *all* of the wavelet peaks in the control regions. Even in this extreme case, a significant CSP detection remains in the inner Galaxy (see text for details).

simulations for a MSP thick-disk population with parameters from Ref. [30], namely $n \propto \exp(-R/R_s) \exp(-|z|/z_s)$, with $R_s = 5$ kpc and $z_s = 1$ kpc (this is more compact in terms of radius, and extends to somewhat higher latitude than what is found by Ref. [38], which makes our results more conservative). We use the above luminosity function with $L_{\max} = 7 \times 10^{34} \text{ erg s}^{-1}$ in the simulation.

We add the deviations from the null-hypothesis that we obtain from this MC as additional (negative or positive) contributions to the peak expectation values μ_{ij} in Eq. (3) in the main text, and repeat the CSP fit to inner Galaxy. We repeat this procedure in all of the control ROIs used in Fig. S-4, reweighting the thick-disk contribution properly according to the longitudinal distance from the Galactic center, while assuming that the fitted CSP is centered in the control ROIs like above. We adjust the number of disk sources such that *all* wavelet peaks in the control regions are absorbed by the thick-disk population *alone* (we increase the source number until the TS values become approximately zero). Even in this extreme case, we find that in the inner Galaxy a clear excess of wavelet peaks remains above the thick-disk background, and it is absorbed by the CSP. The corresponding TS values are shown in Fig. S-12 (note that here we kept the MSP-like unassociated 3FGL sources unmasked; masking them would remove the excess at $5 \leq S \leq 10$, while leaving lower significance wavelet peaks mostly untouched).

We expect that in reality, the impact of the MSP thick-disk population in the inner Galaxy is likely much weaker. Additional contributions from extragalactic sources or young pulsars are expected to be responsible for part of the wavelet peaks in the control regions, while being less strongly enhanced towards the center. We present a systematic study of all relevant contributions in a forthcoming paper.